Bright-field cell image segmentation by principal component pursuit with an Ncut penalization

Chen, Yuehuan, Wan, Justin

Yuehuan Chen, Justin W. L. Wan, "Bright-field cell image segmentation by principal component pursuit with an Ncut penalization," Proc. SPIE 9413, Medical Imaging 2015: Image Processing, 94133F (20 March 2015); doi: 10.1117/12.2081637

SPIE.

Event: SPIE Medical Imaging, 2015, Orlando, Florida, United States

Bright-field Cell Image Segmentation by Principal Component Pursuit with an Ncut Penalization

Yuehuan Chen[a], Justin W.L. Wan[a,b]

[a]Centre for Computational Mathematics in Industry and Commerce, University of Waterloo, Ontario, Canada; [b]David R. Cheriton School of Computer Science, University of Waterloo, Ontario, Canada

ABSTRACT

Segmentation of cells in time-lapse bright-field microscopic images is crucial in understanding cell behaviours for oncological research. However, the complex nature of the cells makes it difficult to segment cells accurately. Furthermore, poor contrast, broken cell boundaries and the halo artifact pose additional challenges to this problem. Standard segmentation techniques such as edged-based methods, watershed, or active contours result in poor segmentation. Other existing methods for bright-field images cannot provide good results without localized segmentation steps. In this paper, we present two robust mathematical models to segment bright-field cells automatically for the entire image. These models treat cell image segmentation as a background subtraction problem, which can be formulated as a Principal Component Pursuit (PCP) problem. Our first segmentation model is formulated as a PCP with nonnegative constraints. We exploit the sparse component of the PCP solution for identifying the cell pixels. However, there is no control on the quality of the sparse component and the nonzero entries can scatter all over the image, resulting in a noisy segmentation. The second model is an improvement of the first model by combining PCP with spectral clustering. Seemingly unrelated approaches, we combine the two techniques by incorporating normalized-cut in the PCP as a measure for the quality of the segmentation. These two models have been applied to a set of C2C12 cells obtained from bright-field microscopy. Experimental results demonstrate that the proposed models are effective in segmenting cells from bright-field images.

Keywords: bright-field images, image segmentation, normalized cut, principal component pursuit

1. INTRODUCTION

Monitoring cell activities is a crucial step in oncological study. Biologists use the time-lapse microscopies taken in a restricted time interval to observe the different cell behaviors under different drug treatments. An accurate segmentation is, therefore, needed for the analysis of cell numbers, cell shapes, and cell movements. This task can be performed easily in human vision system. However, the massive amount of images from laboratories necessitates the use of computer to facilitate the segmentation.

In order to capture the cell cycle progress, biologists have adopted different types of microscopy. Fluorescent and bright-field microscopy are two most common techniques. Fluorescent images typically show distinct appearance of the cells, but they often only capture the nuclei.[1] Moreover the gene introduced in the cells may have undesirable effects on the cell behaviors. Bright-field microscopy, on the other hand, is much less invasive and can show both the nucleus and cytoplasm.[2] However, the low cell-to-background contrast, and the broken cell boundaries resulted from the artifacts (halo) of the light microscopy make the segmentation of bright-field images much harder than that of fluorescent images. Classical image segmentation methods such as edge-based methods, watershed methods, and active contour methods usually can only capture the halo around the cells.[3] Spectral clustering based methods have been applied to the bright-field cell segmentation but mostly for images with a single cell.[4] Some local-global methods, which segment single cells individually and then combine every piece of segmented cells together, were proposed to address the issue.[5] However, these methods can be hard to implement, and create overheads in application. In this paper, we develop two robust mathematical models to segment bright-field cell images without localized segmentation steps.

For further information, please contact Yuehuan Chen: y225chen@uwaterloo.ca, or Justin W.L. Wan: justin.wan@uwaterloo.ca.

Medical Imaging 2015: Image Processing, edited by Sébastien Ourselin, Martin A. Styner, Proc. of SPIE Vol. 9413, 94133F · © 2015 SPIE · CCC code: 1605-7422/15/$18 · doi: 10.1117/12.2081637

2. METHODOLOGY

Bright-field segmentation can be considered as a problem of identifying the moving cells over time. We will propose two cell segmentation approaches based on this idea. In the first approach, segmentation is formulated as a PCP problem, where the sparse component from the PCP is considered as indicator vector to classify cell pixels and background pixels. In the second approach, we improve the first model by combining the PCP with spectral clustering.

2.1 Cell segmentation as a PCP problem

PCP was introduced by Candes *et al.* (2009)[6] as a method for background subtraction in video analysis. Frames in a video surveillance system form the columns of a data matrix M. PCP seeks a decomposition of M such that $M = L + S$, where columns of L correspond to the static background, and the columns of S correspond to the moving objects. In our case, each microscopic image taken at consecutive time is stored as a column of an $m \times n$ data matrix M, where m is the product of the image dimensions and n is the number of cell images. The PCP problem is formulated as a convex optimization problem which minimizes the sum of the nuclear norm of the low-rank component L and the ℓ_1 norm of the sparse component S subject to linear constraints:

$$\begin{aligned} \min_{L,S} \quad & \|L\|_* + \lambda \|S\|_1 \\ \text{subject to} \quad & L + S = M. \end{aligned} \tag{1}$$

Here, L recovers the static background, and S recovers the cells. However, due to noise, the pixel intensities of the dark background fluctuate. As a result, the recovered sparse component S is noisy with some of the entries being negative and small magnitude in order to force L to be low-rank in the decomposition. As S is supposed to represent the cell objects in an image, it is not desirable to have negative entries. Thus, we propose modifying the problem with extra non-negative constraints:

$$\begin{aligned} \min_{L,S} \quad & \|L\|_* + \lambda \|S\|_1 \\ \text{subject to} \quad & L + S = M, \\ & L = L+,\ S = S+, \\ & L+ \geq 0,\ S+ \geq 0. \end{aligned} \tag{2}$$

Two auxiliary variables, $S+$ and $L+$, are introduced so that we can solve (2) by the alternating direction method of multipliers (ADMM) similar to Candes *et al.* (2009). The augmented Lagrangian of (2) is

$$\begin{aligned} & \mathcal{L}(L, S, L+, S+, Y, Z, Q) = \\ & \|L\|_* + \lambda \|S\|_1 + \langle Y, M - L - S \rangle + \frac{\mu}{2} \|M - L - S\|_F^2 + \\ & \langle Z, L - L+ \rangle + \langle Q, S - S+ \rangle + \frac{\gamma}{2} \|L - L+\|_F^2 + \frac{\gamma}{2} \|S - S+\|_F^2. \end{aligned} \tag{3}$$

The strategy is to minimize (3) one variable at a time. Since the non-negative constraints are applied to $L+$ and $S+$ only, the updates of L and S are similar to those of the regular PCP in Candes et al. (2009). The dual variable Y, Z, and Q are updated using gradient descent. For the updates of $L+$ and $S+$, we consider the following problems:

$$\begin{aligned} \min_{L+} \quad & \langle Z, L - L+ \rangle + \frac{\gamma}{2} \|L - L+\|_F^2 \\ \text{subject to} \quad & L+ \geq 0, \end{aligned}$$

and

$$\begin{aligned} \min_{S+} \quad & \langle Q, S - S+ \rangle + \frac{\gamma}{2} \|S - S+\|_F^2 \\ \text{subject to} \quad & S+ \geq 0. \end{aligned}$$

The above problems are non-negative quadratic programmings. We follow similar approaches as Sun (2014)[7] to update $L+$ and $S+$:

$$\begin{aligned} L+ &= \max(L + \gamma^{-1} Z, 0), \\ S+ &= \max(S + \gamma^{-1} Z, 0). \end{aligned}$$

The columns of the sparse component S will be used as indicator vectors for the n images such that the zero entries indicate the background and the nonzero entries indicate the cells. However, while S is a sparse matrix with non-negative entries, it may have nonzero entries distributed everywhere. In fact we have observed that there are some zero entries inside the cell bodies, and some nonzero entries in the background. These are the misclassified points in our case. Some post processing is needed to clean up the results, and to remove the scattered noise in the background. In the second model, we propose a more robust variation such that the post processing is not required. The principal steps involved in solving a PCP with non-negative constraints is outlined in Table 1.

Table 1: Non-negative Robust Principal Component Analysis for image segmentation.

Algorithm 1	
1.	Initialize $S = L = S+ = L+ = Y = Z = Q = 0$ and $\mu, \lambda, \gamma > 0$
2.	while not converge do
	i) $L = \mathcal{D}^*_{(\mu+\gamma)^{-1}}(\mu(\mu+\gamma)^{-1}M - \mu(\mu+\gamma)^{-1}L + (\mu+\gamma)^{-1}Y + \gamma(\mu+\gamma)^{-1}(L+) - (\mu+\gamma)^{-1}Z)$
	ii) $S = \mathcal{S}^\dagger_{\lambda(\mu+\gamma)^{-1}}(\mu(\mu+\gamma)^{-1}M - \mu(\mu+\gamma)^{-1}L + (\mu+\gamma)^{-1}Y + \gamma(\mu+\gamma)^{-1}(S+) - (\mu+\gamma)^{-1}Q)$
	iii) $L+ = \max(L + \gamma^{-1}Z, 0)$
	iv) $S+ = \max(S + \gamma^{-1}Z, 0)$
	v) $Y = Y + \mu(M - L - S)$
	vi) $Z = Z + \gamma(L - L+)$
	vii) $Q = Q + \gamma(Q - Q+)$
3.	end while
4.	output S

2.2 Cell segmentation as a PCP problem with normalized-cut penalization

The idea is to incorporate spectral clustering in the PCP model. Notice that both spectral clustering and PCP can be formulated as minimization problems. Spectral clustering minimizes the graph-cut which imposes penalty on the "goodness" of an image segmentation. Let $L^{(S_j)}$ be the graph Laplacian matrix corresponding the jth cell image, and X_j be the indicator vector whose zero-crossing indicates the segmentation. The normalized-cut, $X_j^T L^{(S_j)} X_j$, is proportional to the edge weights between different segments, so the correct segmentation can be founded by the minimizer of the normalized-cut. Since the jth column of the sparse component from the PCP also determines the segmentation of the jth cell image, we propose solving the following problem:

$$\min_{L,S,X,A} \quad \|L\|_* + \lambda_1 \|S\|_1 + \frac{\lambda_2}{2} \sum_{j=1}^{n} {X_j}^T L^{(S_j)} X_j + \sum_{j=1}^{n} \sum_{i=1}^{m} A_{ij}^+$$

*The symbol $\mathcal{D}_\lambda$ denotes the singular value thresholding operator $\mathcal{D}_\lambda(X) = U\mathcal{S}_\lambda(\Sigma)V^*$, where $X = U\Sigma V^*$.

†The symbol $\mathcal{S}_\lambda$ denotes the shrinkage operator $\mathcal{S}_\lambda(x) = sign(x)\max(|x| - \lambda, 0)$.

$$\begin{aligned} \text{subject to} \quad & L + S = M, \\ & A = \mathbf{1} - X sign(|S| - \epsilon), \\ & \mathbf{1}^T X_j = 0, j = 1, ..., n, \\ & X_j^T X_j = 1, j = 1, ..., n, \end{aligned} \tag{4}$$

where A^+ is the positive part of A and ϵ is a small parameter. The jth column of A is an auxiliary variable to measure the discrepancy between the segmentation defined by X_j and the segmentation defined by S_j. The constraint on A links the sparse component S from the PCP with the indicator matrix X from the normalized-cut. The last two constraints are similar to those in spectral clustering.

As in above, we solve this optimization problem by ADMM. Four dual variables (Y, Z, α, β) and a parameter μ are introduced in the augmented Lagrangian $\mathbf{L}(L, S, X, A, Y, Z, \alpha, \beta)$. The dual variables are updated using a gradient descent method. The updates of L and S are similar to (2) except that we need to solve a nonlinear equation (due to the constraints given by A) instead of a linear equation to update S. While keeping the other unknowns in $\mathbf{L}$ fixed, the solution of

$$A_{ij} = \underset{A_{ij}}{\text{argmin}} \ \mathbf{L},$$

is given by $\mathbf{S}_{\frac{1}{m\mu}}(\mathbf{1} - X_j sign(|S_j| - \epsilon) + \frac{Z_j}{\mu})$, where $\mathbf{S}_\lambda(\gamma)$ for some parameters λ and γ as defined in Proposition 1 of Ye, Chen, Xie (2011).[8]

Let $b_j = \mathbf{1} - A_j$, and $D_j = Diag(sign(|S_j| - \epsilon))$. We can write the unconstrained problem

$$X_j = \underset{X_j}{\text{argmin}} \ \mathbf{L} \tag{5}$$

as a constrained problem[‡]

$$\begin{aligned} \min_{X_j, j=1...n} \quad & \frac{\lambda_2}{2} {X_j}^T L^{(S_j)} X_j + \frac{\mu}{2} X_j^T D_j^T D_j X_j - (Z_j^T D_j + b_j D_j) X_j \\ \text{subject to} \quad & \mathbf{1}^T X_j = 0, j = 1, ..., n, \\ & X_j^T X_j = 1, j = 1, ..., n. \end{aligned} \tag{6}$$

We can reformulate (6) by introducing an auxiliary variable $Q_j = -(Z_j^T D_j + b_j^T D_j) X_j$ and a sufficiently large constant ν so that $(\nu I - \frac{\lambda_2}{2} L^{(S_j)} - \frac{\mu}{2} D_j^T D_j)$ is positive definite:

$$\begin{aligned} \max_{X_j, j=1...n} \quad & X_j^T (\nu I - \frac{\lambda_2}{2} L^{(S_j)} - \frac{\mu}{2} D_j^T D_j) X_j \\ \text{subject to} \quad & \mathbf{1}^T X_j = 0, j = 1, ..., n, \\ & X_j^T X_j = 1, j = 1, ..., n, \\ & -(Z_j^T D_j + b_j^T D_j) X_j = Q_j. \end{aligned} \tag{7}$$

The solution of (7) is approximated by the solution of an Affinely Constrained Rayleigh Quotients (ACRQ) problem which can be solved efficiently by the algorithm proposed in Cour, Srinivasan, Shi (2007).[9] After the optimization problem is solved, we can use X_j as an indicator vector to obtain the segmentation of the jth image. We summarize this method in Table 2.

[‡]Problem (5) and (6) are not equivalent, but the constrained problem (6) gives a better approximation to (4).

Table 2: Robust Principal Component Analysis with normalized-cut penalization for image segmentation.

Algorithm 2	
1.	Initialize $L = S = X = Y = A = Z = G = 0$ and $\mu, \lambda_1, \lambda_2 > 0$
2.	while not converge do
	i) $L = \mathcal{D}_{\mu^{-1}}(M - S + \mu^{-1}Y)$
	ii) Solve $\mathbf{L}'(S) = 0$, where $\mathbf{L}$ is the augmented Lagrangian
	iii) $Y = Y + \mu(M - L - S)$
	iv) ${b_j}^{\S} = \mathbf{1} - A_j, D_j = Diag(H^{\P}(S_j))$
	v) Solve (7) as described in Cour, Srinivasan, Shi (2007)
	vi) $Q_j = \frac{-1}{\mu} - \frac{G_j}{\mu} - ({Z_j}^T D_j + {b_j}^T D_j)X_j$
	vii) $G_j = G_j + \mu(Q_j - ({Z_j}^T D_j + {b_j}^T D_j)X_j)$
	viii) $A_j = S_{\frac{1}{m\mu}}(1 + \frac{Z_j}{\mu} - X_j H(S_j))$
	ix) $Z_j = Z_j + \mu(1 - X_j H(S_j) - A_j)$
3.	end while
4.	output X

3. NUMERICAL RESULTS

We present the segmentation results on a set of C2C12 cell images from the Genomic Laboratory at McGill University. The algorithms were implemented using MATLAB. Due to computational time limitation, the original input images were down-sampled to 300×300 for the experiments. We apply the two models on a 90000×120 data matrix M using $\lambda = \frac{2}{\sqrt{m}}$, $\mu = 0.25\text{mean}(M_{ij})$ for Model 1, and $\lambda_1 = \lambda_2 = \frac{1}{\sqrt{m}}$, $\mu = 0.25\text{mean}(M_{ij})$ for Model 2.

Figure 1 shows the segmentation results obtained from Model 1 and Model 2. The columns are four frames of a cell image sequence corresponding to the beginning, middle stage, and after of a cell division. The images in the first row are the input images. The second row shows the indicator matrices obtained from Model 1. Morphological operations are performed to obtain the compact segmentation results shown in the third row. The fourth row shows the indicator matrices obtained from Model 2. No post-processing is required in this model. The fifth row shows the segmentation results by Model 2. These two models both can capture most of the cells in the images, but Model 2 gives more precise segmentation results. For instance, consider the group of cells near the center of the image. Model 1 can locate most parts of the cells, but the resulting cell boundaries tend to over segment. Model 2, on the other hand, gives a smoother boundary that fits better with the cells.

We also present some validation results of the proposed models. The ground truth of ten image frames are obtained by manual segmentation. Figure 2 shows the true positive, true negative, false positive, and false negative rates given by the two models. On the average, the corresponding rates are 0.84, 0.94, 0.055, and 0.16 respectively for Model 1, and 0.87, 0.95, 0.047, 0.13 for Model 2. They both show good accuracy with Model 2 slightly better than Model 1.

4. CONCLUSION

In this work, we proposed two image segmentation models based on PCP. The first model treats the segmentation problem as a PCP with non-negative constraints, where the sparse component is used for the segmentation. The second model combines the PCP with spectral clustering in a minimization framework. The output vectors from the corresponding ACRQ problems are used for the segmentation. These two models can capture the boundaries of all cells in a microscopic image, but the second model is more robust and no post processing is required to obtain good segmentation results.

[§]The number j denotes the column index.

[¶]The function H is a smooth approximation of $sign(|S_j| - \epsilon)$, e.g., $tanh(|S_j| - \epsilon)$.

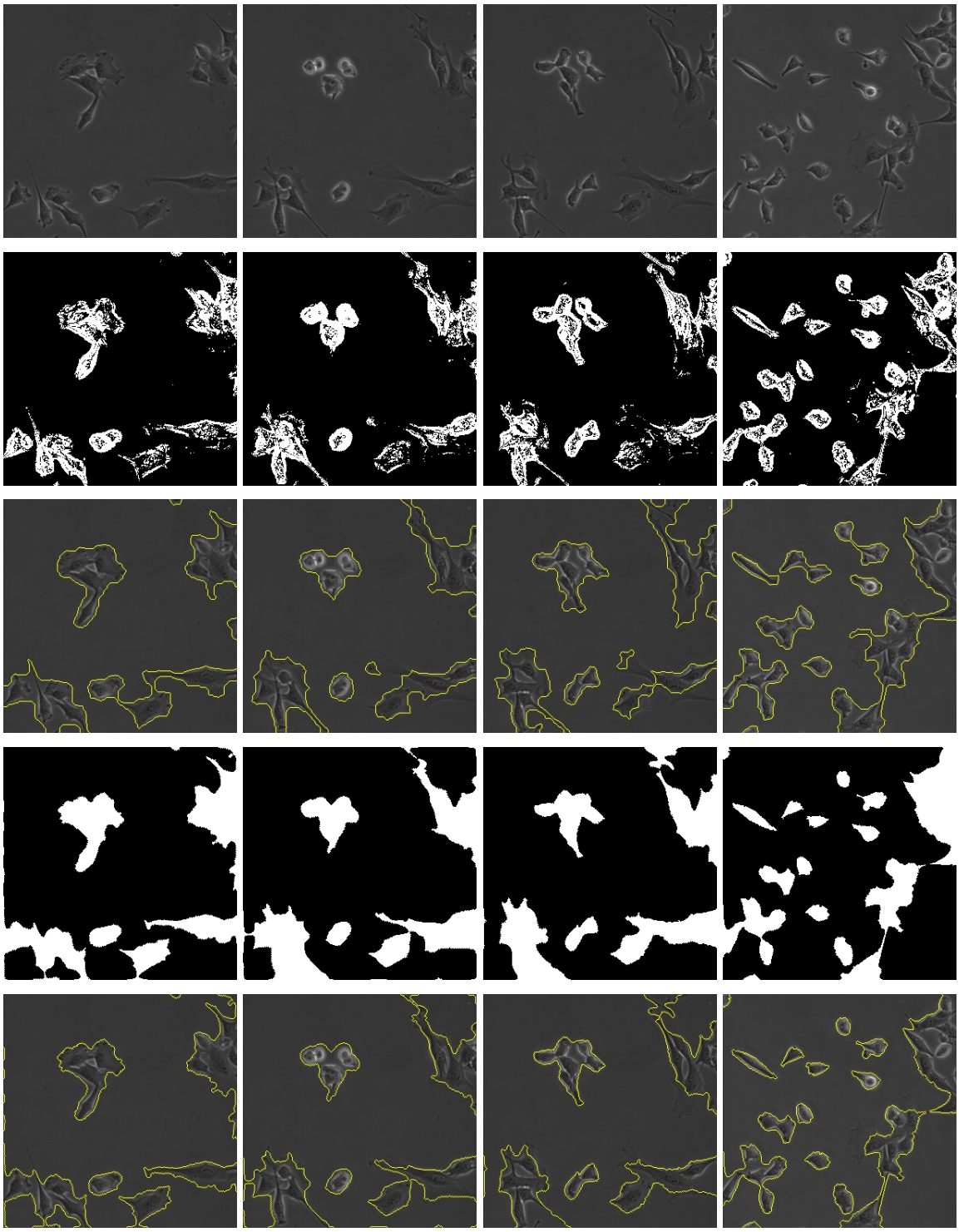

Figure 1: Segmentation results of the cell image frame (first row) given by Model 1 (third row) and Model 2 (fifth row).

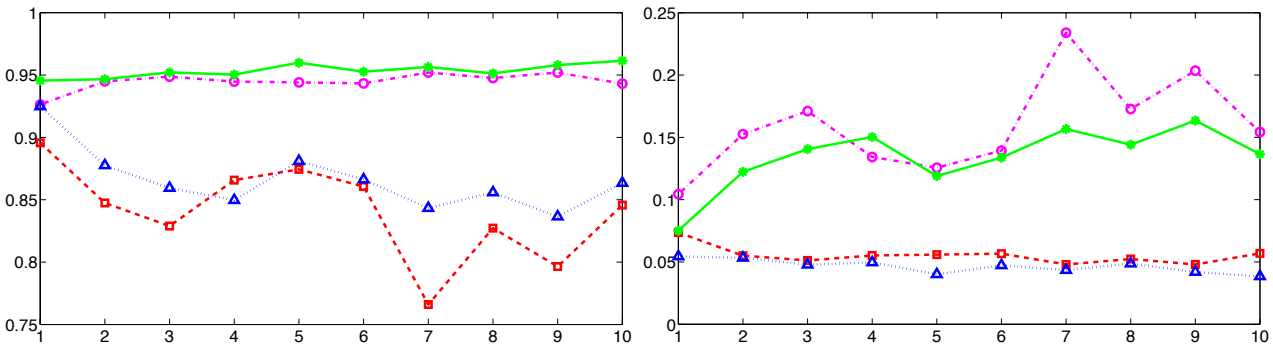

Figure 2: (Left) True positive rates (Model 1: dashed red, Model 2: dotted blue) and true negative rates (Model 1: dashdot magenta, Model 2: solid green), (right) false positive rates (Model 1: dashed red, Model 2: dotted blue) and false negative rates (Model 1: dashdot magenta, Model 2: solid green).

ACKNOWLEDGMENTS

The authors would like to thank Robert Sladek and Haig Djambazian from the Department of Medicine and Human Genetics at McGill University for the provision of the C2C12 microscopy images. This work was supported by the National Sciences and Engineering Research Council of Canada.

REFERENCES

[1] Dzyubachyk, O., van Cappellen, W., Esser, J., Niessen, W., and Meijering, E., "Advanced level-set-based cell tracking in time-lapse fluorescence microscopy," *IEEE Transactions on Medical Imaging* **29**, 852–867 (2010).

[2] Korzynska, A., Strojny, W., Hoppe, A., Wertheim, D., and Hoser, P., "Segmentation of microscope images of living cells," *Pattern Anal. Appl.* **10**(4), 301–319 (2007).

[3] Tse, T., Bradbury, L., Wan, J., Djambazian, H., Sladek, R., and Hudson, T., "A combined watershed and level set method for segmentation of brightfield cell images," *Proceedings of SPIE Symposium on Medical Imaging: Image Processing* **7259** (2009).

[4] Bradbury, L. and Wan, J., "A spectral K-means approach to bright-field cell image segmentation," *32nd Annual International Conference of the IEEE EMBS* (2010).

[5] Kang, S. and Wan, J., "A multiscale graph cut approach to bright-field multiple cell image segmentation using a Bhattacharyya measure," *Proceedings of SPIE Symposium on Medical Imaging: Image Processing* **8669** (2013).

[6] Candès, E. J., Li, X., Ma, Y., and Wright, J., "Robust principal component analysis?," *Journal of the ACM (JACM)* **58**(3), 11 (2011).

[7] Sun, D. L. and Fevotte, C., "Alternating direction method of multipliers for non-negative matrix factorization with the beta-divergence," in [*IEEE International Conference on Acoustic, Speech and Signal Processing (ICASSP)*], 6201–6205 (2014).

[8] Ye, G.-B., Chen, Y., and Xie, X., "Efficient variable selection in support vector machines via the alternating direction method of multipliers," in [*International Conference on Artificial Intelligence and Statistics*], 832–840 (2011).

[9] Cour, T., Srinivasan, P., and Shi, J., "Balanced graph matching," *Advances in Neural Information Processing Systems* **19**, 313–320 (2006).

[10] Boyd, S., Parikh, N., Chu, E., Peleato, B., and Eckstein, J., "Distributed optimization and statistical learning via the alternating direction method of multipliers," *Foundations and Trends® in Machine Learning* **3**(1), 1–122 (2011).

[11] Dougherty, G., [*Digital image processing for medical applications*], Cambridge University Press (2009).

[12] Gander, W., "Least squares with a quadratic constraint," *Numerische Mathematik* **36**(3), 291–307 (1980).

[13] Goldstein, T. and Osher, S., "The split bregman method for l1-regularized problems," *SIAM Journal on Imaging Sciences* **2**(2), 323–343 (2009).

[14] Kim, H. and Park, H., "Sparse non-negative matrix factorizations via alternating non-negativity-constrained least squares for microarray data analysis," *Bioinformatics* **23**(12), 1495–1502 (2007).

[15] Lai, R. and Osher, S., "A splitting method for orthogonality constrained problems," *Journal of Scientific Computing* **58**(2), 431–449 (2014).

[16] Shi, J. and Malik, J., "Normalized cuts and image segmentation," *IEEE Transactions on Pattern Analysis and Machine Intelligence* **22**(8), 888–905 (2000).

[17] Von Luxburg, U., "A tutorial on spectral clustering," *Statistics and computing* **17**(4), 395–416 (2007).

[18] Ye, G.-B. and Xie, X., "Split bregman method for large scale fused lasso," *Computational Statistics & Data Analysis* **55**(4), 1552–1569 (2011).